Pakistan Veterinary Journal

ISSN: 0253-8318 (PRINT), 2074-7764 (ONLINE)
DOI: 10.29261/pakvetj/2026.113

RESEARCH ARTICLE

Combined Exposure to Copper Sulfate and Polystyrene Microplastics Alters Intestinal Microbiota Structure and Induces Barrier Damage in Male Mice

Bingxin Lv[1,2†], Hui Zhang[1,2†], Ziqin Zhang[1,2†], Yaao Pan [1,2], Sheng Kang[1,2], Mi Chen[1,2], Xiaoya Li[3], Farid S. Ataya[4], Runbo Luo[5] and Zhenyu Chang[1,2*]

[1]Key Laboratory of Clinical Veterinary Medicine in Xizang, Xizang Agriculture and Animal Husbandry University, Xizang, People's Republic of China; [2]Key Laboratory for Prevention and Control of Hydatid Disease in Xizang (Co-constructed by Ministry and Province), Ministry of Agriculture and Rural Affairs, College of Animal Science, Xizang Agricultural and Animal Husbandry University, Linzhi, Xizang 860000; [3]Linzhi Municipal Bureau of Agriculture and Rural Affairs, Linzhi, 860000, China; [4]Department of Biochemistry, College of Science, King Saud University, P.O. Box 2455, Riyadh 11451, Saudi Arabia; [5]College of Veterinary Medicine, Nanjing Agricultural University, Nanjing 210095, P. R. China. †These authors contributed equally to this article.
*Corresponding author: zychang2014@sina.com

ARTICLE HISTORY (26-425)

Received: April 18, 2026
Revised: May 26, 2026
Accepted: May 28, 2026
Published online: May 30, 2026

Key words:
Combined exposure
Intestinal injury
Copper sulfate
Polystyrene microplastics

ABSTRACT

This study explores the intestinal toxicity of combined copper sulfate (Cu) and polystyrene microplastics (PS) exposure in male mice. Histopathological examination, intestinal barrier function assessment, 16S rRNA sequencing, and transcriptome analysis were performed to explore the underlying mechanisms. The results showed that combined exposure significantly decreased ileal villus height, aggravated tissue damage, and evidently suppressed the synthesis of tight junction structural proteins, including claudin, ZO-1, and occludin. Analysis of 16S rRNA sequencing indicated that combined exposure markedly altered intestinal microbial structure, leading to a reduction of beneficial bacteria, enrichment of inflammation-related bacteria, and significant intestinal flora remodeling. Transcriptome profiling identified a total of 4026 differentially expressed genes (DEGs) in the co-exposure group, with 3226 specific DEGs, which was significantly higher than that in the single exposure groups. Functional enrichment analyses based on GO and KEGG databases demonstrated that DEGs were mainly involved in inflammation-associated signaling pathways. Among these were antigen presentation, IgA immune network, development and differentiation of T cells, and NOD-like receptor signaling axis. In conclusion, combined exposure to Cu and PS exerts obvious combined effects on intestinal flora disturbance and intestinal barrier damage in mice.

To Cite This Article: Lv B, Zhang H, Zhang Z, Pan Y, Kang S, Chen M, Li X, Ataya FS, Luo R, and Chang Z, 2026. Combined exposure to copper sulfate and polystyrene microplastics alters intestinal microbiota structure and induces barrier damage in male mice. Pak Vet J, 46(5): 1264-1275. http://dx.doi.org/10.29261/pakvetj/2026.113

INTRODUCTION

The intestinal microbiota, often referred to as the 'second genome' of humans, constitutes an essential component of the intestinal barrier and is regarded as a critical target for heavy metal toxicity (Hou *et al*., 2025). Exposure to heavy metals alters intestinal microbiota composition, a critical mediating factor that influences heavy metal bioavailability and systemic toxicity in the host (Liu *et al*., 2023). Heavy metals such as lead, cadmium, and arsenic can induce intestinal damage through oxidative stress, inflammatory responses, and microbiota dysbiosis (Yang *et al*., 2023; Li *et al*., 2026). Copper, an essential trace element with dual properties as both a nutrient and a potential toxicant, can accumulate substantially in the intestine, warranting particular attention to its intestinal toxic effects (Zhu *et al*., 2026). Studies have shown that copper exposure alters intestinal microbiota α-diversity and β-diversity, lowers the population of specific probiotics and putative SCFA-producing microbial strains, induces intestinal oxidative stress and inflammatory responses, compromises mucosal barrier integrity, and disturbs various metabolic pathways such as lipid and amino acid metabolism, thereby undermining intestinal homeostasis and organismal health (Dai *et al*., 2020; Zhu *et al*., 2024). In addition to heavy metals, polystyrene microplastics (PS-MPs), as ubiquitous environmental pollutants, also exhibit significant intestinal

toxicity. Microplastics can accumulate in the intestine, disrupt intestinal villus structure and epithelial integrity, reduce mucus secretion, enhance oxidative stress and inflammatory responses, and markedly alter intestinal microbiota structure and function (Liang *et al*., 2021; Wen *et al*., 2022; Chen *et al*., 2023; Zhang *et al*., 2023). This toxicity is particle size-, dose-, and time-dependent; smaller particles more readily penetrate barriers and inflict severe damage. Microplastic-induced intestinal injury is exacerbated under susceptible or inflammatory states, identifying these pollutants as potential environmental risk factors for inflammatory bowel disease (Huang *et al*., 2022; Lv *et al*., 2023).

Previous studies have demonstrated that combined heavy metal and microplastic exposure elicits combined toxic effects, markedly disrupting intestinal microecological homeostasis and exacerbating barrier impairment and metabolic disorders compared with single exposure, wherein intestinal microbiota dysbiosis serves as a critical mediator (Hu *et al*., 2024; Shen *et al*., 2024; Tang *et al*., 2024). While the intestinal toxicity of copper and microplastics alone has been documented, the integrated effects of their co-exposure on mammalian intestine remain poorly characterized. Specifically, the consequences for gut microbiota, barrier integrity, and molecular responses in male individuals require further systematic investigation.

Using male mice as a model, this study systematically assessed the impacts of individual and combined copper sulfate and PS-MPs exposure on gut microbiota composition, intestinal histopathology, and transcriptomic signatures. The objectives were to clarify the toxic effects induced by co-exposure and establish a theoretical foundation for health risk assessment of environmental co-exposure scenarios.

MATERIALS AND METHODS

Animals and experimental housing conditions: Twenty-four male C57BL/6J mice aged 6 weeks (weighing 20–22g) were purchased from Guangdong Zhiyuan Biomedical Technology Co., Ltd. (Guangzhou, China) and maintained at the Experimental Animal Center of South China Agricultural University. Housing conditions consisted of a temperature of 22–24°C, 50±10% relative humidity, and a 12-hour light-dark cycle, with ad libitum access to food and water. All animal experiments were performed in compliance with relevant ethical regulations.

Animal grouping: After a one-week acclimation phase, the mice were randomly divided into four groups (n=6 each) according to body weight: control, Cu, PS, and Cu+PS.

Preparation of test solutions and animal treatment: Preparation of test solutions: $CuSO_4$ working solution (20mg/mL) and PS-MP working suspension (6mg/mL) were freshly prepared in ultrapure water before each administration. Anhydrous $CuSO_4$ powder was dissolved directly in ultrapure water, and the original PS-MP suspension (2.5% w/v) was diluted to the target concentration. All preparations were thoroughly vortexed to ensure homogeneous dispersion. The exposure concentrations were selected based on relevant published literature for laboratory toxicological research.

Animal treatment: Mice were randomly allocated into four groups and subjected to daily intragastric gavage for 30 consecutive days: the control group received 0.1mL ultrapure water; the $CuSO_4$ and PS-MP groups received 0.1mL of the corresponding working solution or suspension, respectively; and the combined group received 0.2mL of an equal-volume mixture of $CuSO_4$ and PS-MP solutions. All gavage procedures were conducted under identical conditions.

Tissue collection: Twenty-four hours after the final administration, mice were euthanized by cervical dislocation, and tissue specimens were immediately harvested for subsequent analyses.

Intestinal content sampling: Following the final gavage, mice were euthanized by cervical dislocation. Intestinal contents were aseptically collected into pre-cooled sterile centrifuge tubes, rapidly frozen in liquid nitrogen, and preserved at −80°C. Ileal tissue was simultaneously collected for histopathological examination.

Histopathological examination: Ileal tissue samples were rinsed with physiological saline, fixed in 10% neutral buffered formalin for 24h, and embedded in paraffin. Sections (4–5μM) were prepared, dewaxed, rehydrated, and stained with hematoxylin and eosin (H&E). After dehydration and clearing, slides were mounted with neutral balsam and examined under a light microscope to document histopathological changes.

Immunohistochemistry for tight junction proteins: Ileal tissue samples were routinely fixed, paraffin-embedded, and sectioned. Following dewaxing and rehydration, sections underwent immunohistochemical staining. After antigen retrieval and blocking, Sections were incubated with antibodies directed against Claudin, ZO-1, and Occludin, followed by secondary antibody binding, DAB chromogen development, and hematoxylin counterstaining. Subsequently, sections were dehydrated, cleared, mounted, and examined under a microscope for semiquantitative analysis of protein expression.

DNA extraction and 16S rRNA gene amplification: Intestinal content DNA was extracted using a stool genomic DNA kit and verified by agarose gel electrophoresis. The V3–V4 hypervariable region of the 16S rRNA gene was amplified by PCR using primers 338F (5'-ACTCCTACGGGAGGCAGCAG-3') and 806R (5' GGACTACHVGGGTWTCTAAT-3'). Following purification, amplicons were adapter-ligated, size-selected, and sequenced on an Illumina platform.

Bioinformatics analysis and taxonomic classification: Raw sequences were quality-filtered to obtain valid reads. After primer trimming with Cutadapt, sequences were denoised, merged, and chimera-removed using the DADA2 algorithm to generate an amplicon sequence variant (ASV) feature table. Taxonomic identification was conducted based on a standard reference database.

Microbiota diversity and community analysis: Microbiota analysis was conducted on the ASV scale. The

Chao1, ACE, Shannon, and Simpson indices were applied to estimate alpha diversity. Beta diversity and intergroup structural differences were evaluated by principal component analysis (PCA) and principal coordinate analysis (PCoA). Differential taxa were identified and their effect sizes estimated using Metastats and linear discriminant analysis (LDA) coupled with LEfSe. Potential functional profiles were predicted and annotated with PICRUSt2 based on the KEGG and COG databases.

Transcriptome sequencing of ileal tissue: Total RNA was extracted from ileal tissue using TRIzol reagent. RNA samples that passed quality control for concentration, purity (A260/A280 ratio), and integrity (RIN value) were selected for library preparation and Illumina sequencing.

Statistical analysis: Statistical analyses were performed using GraphPad Prism 9.5.0, and data are presented as mean ± SEM. Two-group comparisons were assessed by t-test or Mann–Whitney U test, and multiple-group comparisons by one-way ANOVA with Bonferroni post-hoc correction. Statistical significance was set at $P<0.05$. For transcriptomic data, clean reads were obtained after quality filtering, and DEGs were identified using DESeq2 ($|\log_2 FoldChange| > 1$, adjusted $P<0.05$). GO and KEGG enrichment analyses were conducted to predict functional and pathway alterations of DEGs. These enrichment results are in silico predictions and remain experimentally unvalidated. Given the limited sample size (n=6 per group), all findings were interpreted cautiously to avoid overinterpretation.

RESULTS

Intestinal histopathology: Control mice showed intact, regularly arranged villi. Copper sulfate exposure resulted in villus blunting, height reduction, and focal epithelial injury (Fig. 1). PS-MPs alone caused mild architectural distortion and inflammation. Combined exposure produced the most severe damage, including significantly reduced villus height, marked structural disorganization, and epithelial detachment.

Alterations in intestinal tight junction protein expression: The expression of tight junction-related proteins in ileal tissue from each group (Fig. 2). When compared to the control group, the immunohistochemical staining intensity for Claudin, ZO-1, and Occludin was reduced in both the Cu and PS-MPs groups. The most significant decrease was observed in the group exposed to both substances.

Rarefaction curves and Venn diagram analysis: Rarefaction curves and Venn diagrams for each group are shown in Fig. 3A-B. The plateauing of rarefaction curves indicated adequate sequencing depth and reliable representation of true community richness. The Venn diagram revealed 55 shared ASVs across all four groups, with unique ASVs detected in each treatment (control: 8; Cu: 6; PS-MPs: 10; combined: 5), suggesting that different treatments altered the composition of the mouse intestinal microbiota.

Alpha diversity analysis: The ACE and Chao1 indices, which measure community richness, showed a declining trend in the combined exposure group, although this change was not statistically significant (Fig. 3C- F). In contrast, the Simpson and Shannon indices, which indicate community diversity and evenness, were significantly higher in the PS-MPs group compared to the control group ($P<0.05$ for both). Overall, exposure to PS-MPs had a significant impact on alpha diversity, while the combined exposure primarily led to a reduction in richness without resulting in notable changes in diversity.

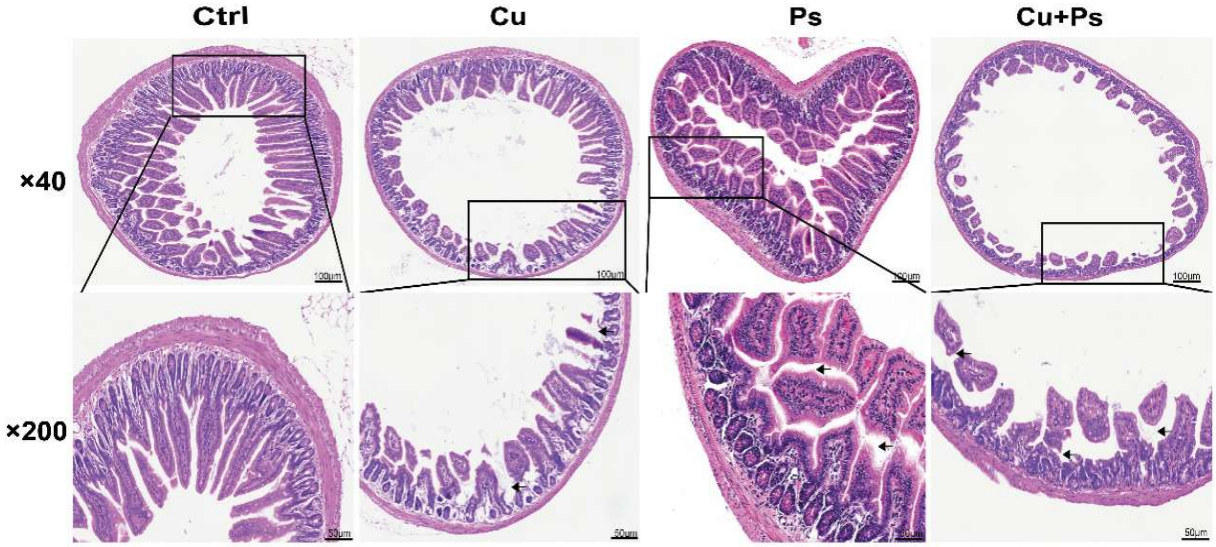

Fig. 1: Representative H&E-stained sections of ileal tissue from control and treated mice. Top row: ×40 magnification; bottom row: ×200. Scale bars: 100μM (×40), 50μM (×200). Arrows denote villous structural changes and inflammatory foci (blunted/thickened villi, edema, or leukocyte infiltration). Cu: copper ions derived from copper sulfate ($CuSO_4$); PS: polystyrene microplastics.

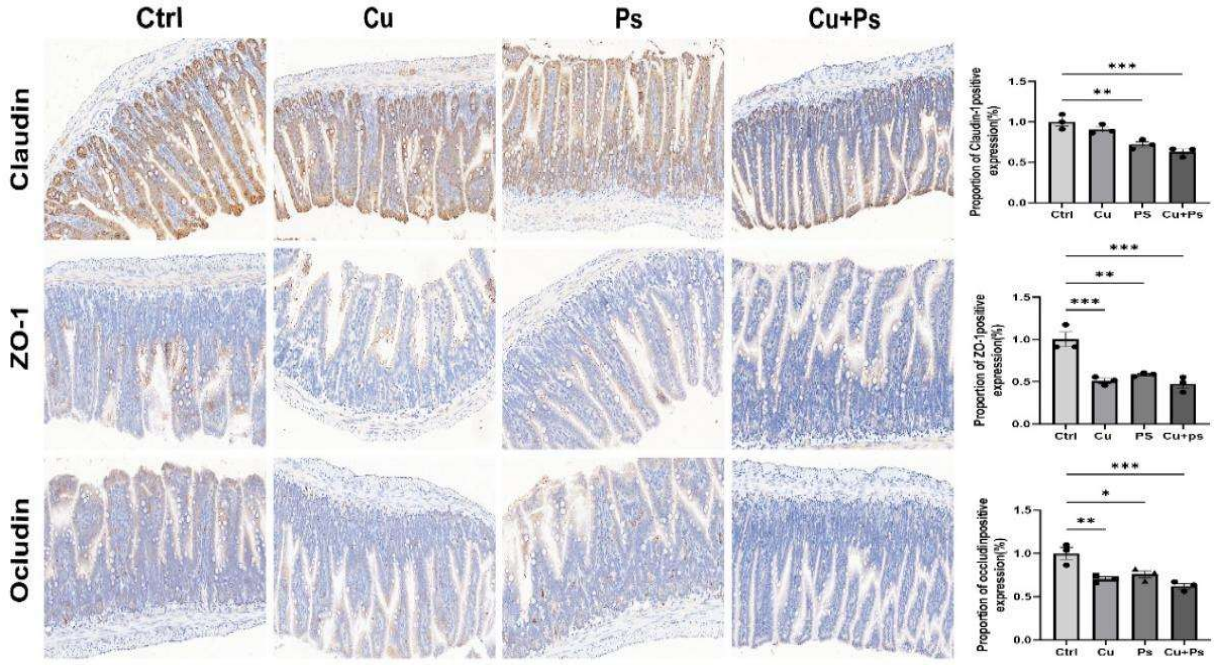

Fig. 2: Immunohistochemical staining and quantitative analysis of Claudin, ZO-1, and Occludin in ileal tissue. Ctrl, control group; Cu group, copper sulfate group; PS, PS-MPs group; Cu+PS, combined exposure group. Right panel: quantitative results of positive staining intensity. Data are presented as mean ± SEM (or SD). Significant differences are represented in the figure (*P<0.05, **P<0.01, ***P<0.001).

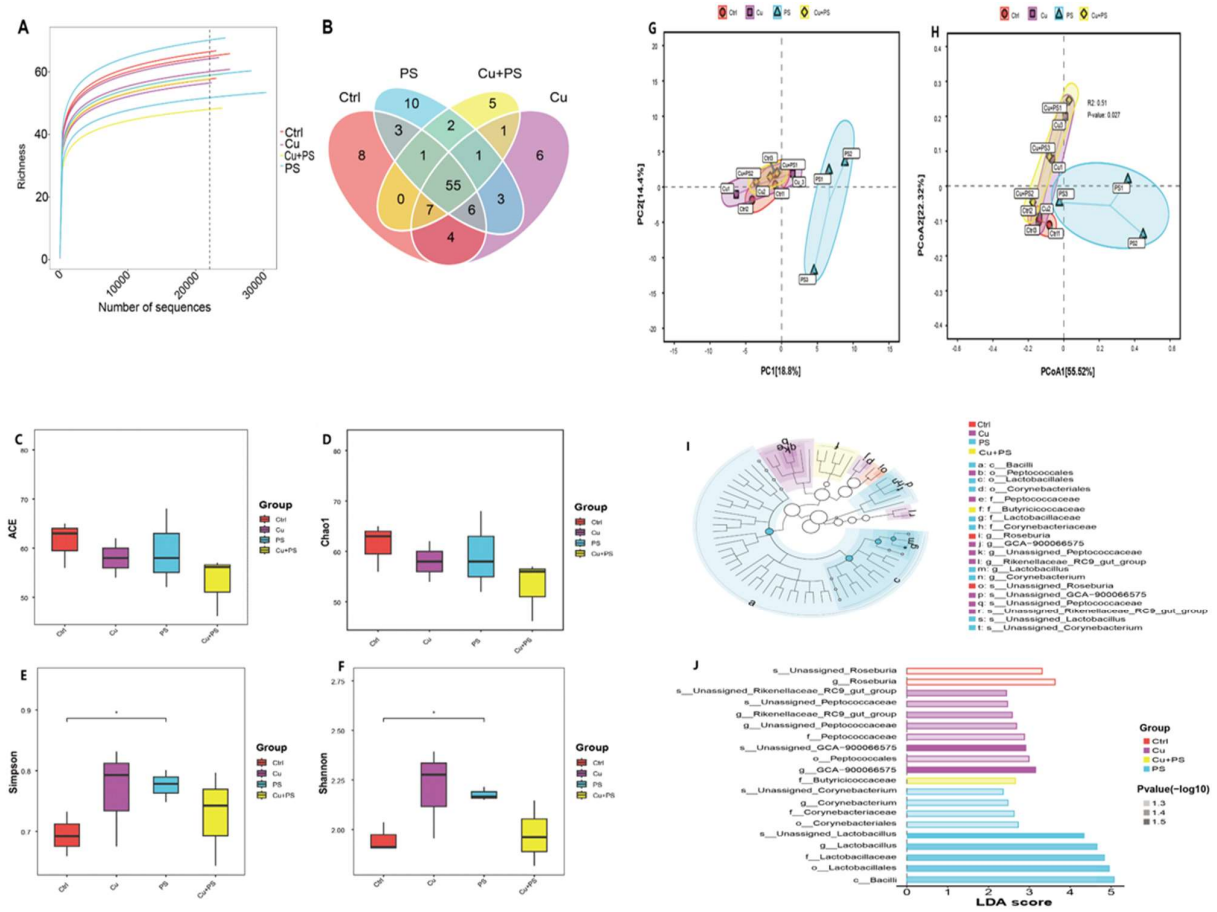

Fig. 3: (A-B): Rarefaction curves and Venn diagrams illustrating the gut microbiota composition in each group. A: Rarefaction curves; B: Venn diagram(C-F) Alpha diversity indices of gut microbiota among each group. C: ACE index; D: Chao1 index; E: Simpson index; F: Shannon index. (G-H): Analysis of beta diversity in gut microbiota for each group. G: Principal component analysis (PCA); H: Principal coordinate analysis (PCoA). (I-J): LEfSe analysis of differentially abundant taxa in intestinal microbiota among groups of mice. I: Cladogram; J: LDA effect size bar plot.

Beta diversity analysis: Principal Component Analysis (PCA) showed a distinct separation among the treatment groups, particularly highlighting that the PS-MPs group was clearly differentiated from the others (Fig. 3G). Additionally, Principal Coordinate Analysis (PCoA) revealed differences in community structure, demonstrating a clear separation of the PS group from the other groups. Notably, there was some overlap among the control, Cu, and combined groups (Fig. 3H). A PERMANOVA analysis based on the PCoA distances indicated statistically significant differences among the groups (R^2=0.51, P=0.027), suggesting that the different treatments influenced the structure of the intestinal microbiota.

Taxonomic composition analysis: The bacterial composition is detailed at the phylum, family, genus, and species levels in Fig. 4. At the phylum level, the dominant groups are Firmicutes, Bacteroidetes, and Verrucomicrobia, with varying relative abundances among the different groups. At the family level, Lachnospiraceae, Lactobacillaceae, and Akkermansiaceae are predominant but show different distributions. At the genus level, the most abundant groups are Lachnospiraceae_ NK4A136_group, Lactobacillus, and Akkermansia, with a notable increase in Clostridia_UCG-014 observed in the combined exposure group. At the species level, the abundance of *Bifidobacterium pseudolongum* increased across all treatment groups. Overall, the combined exposure group demonstrated the most significant changes in microbiota composition across multiple taxonomic levels.

Heatmap analysis of relative abundance of intestinal microbiota at different taxonomic levels: The community abundance heatmap was drawn based on ASV relative abundance (Fig. 5). Analysis of the phylum, family, genus, and species levels revealed distinct differences in microbiota composition among the four groups. The copper-exposed group exhibited enrichment of sulfate-reducing microbiota (e.g., Desulfobacterota, Desulfovibrio); the microplastic group showed decreased abundance of butyrate-producing bacteria; and the combined exposure group displayed significantly reduced abundance of the core probiotics *Bifidobacterium pseudolongum* and *Lactobacillus reuteri*.

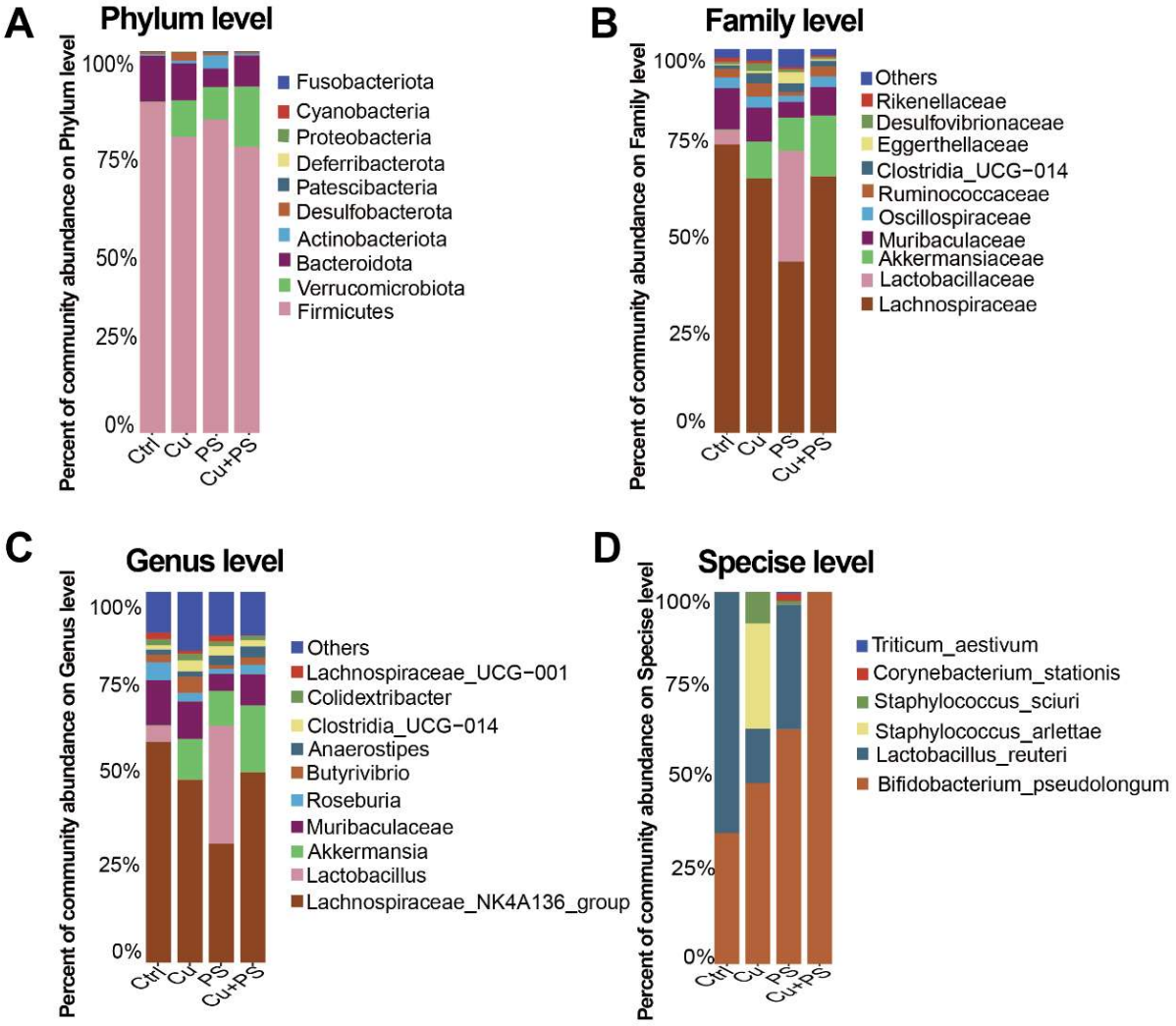

Fig. 4: Composition of intestinal microbiota's relative abundance in each group of mice at phylum, family, genus, and species levels. A: Phylum level; B: Family level; C: Genus level; D: Species level of microbiota composition.

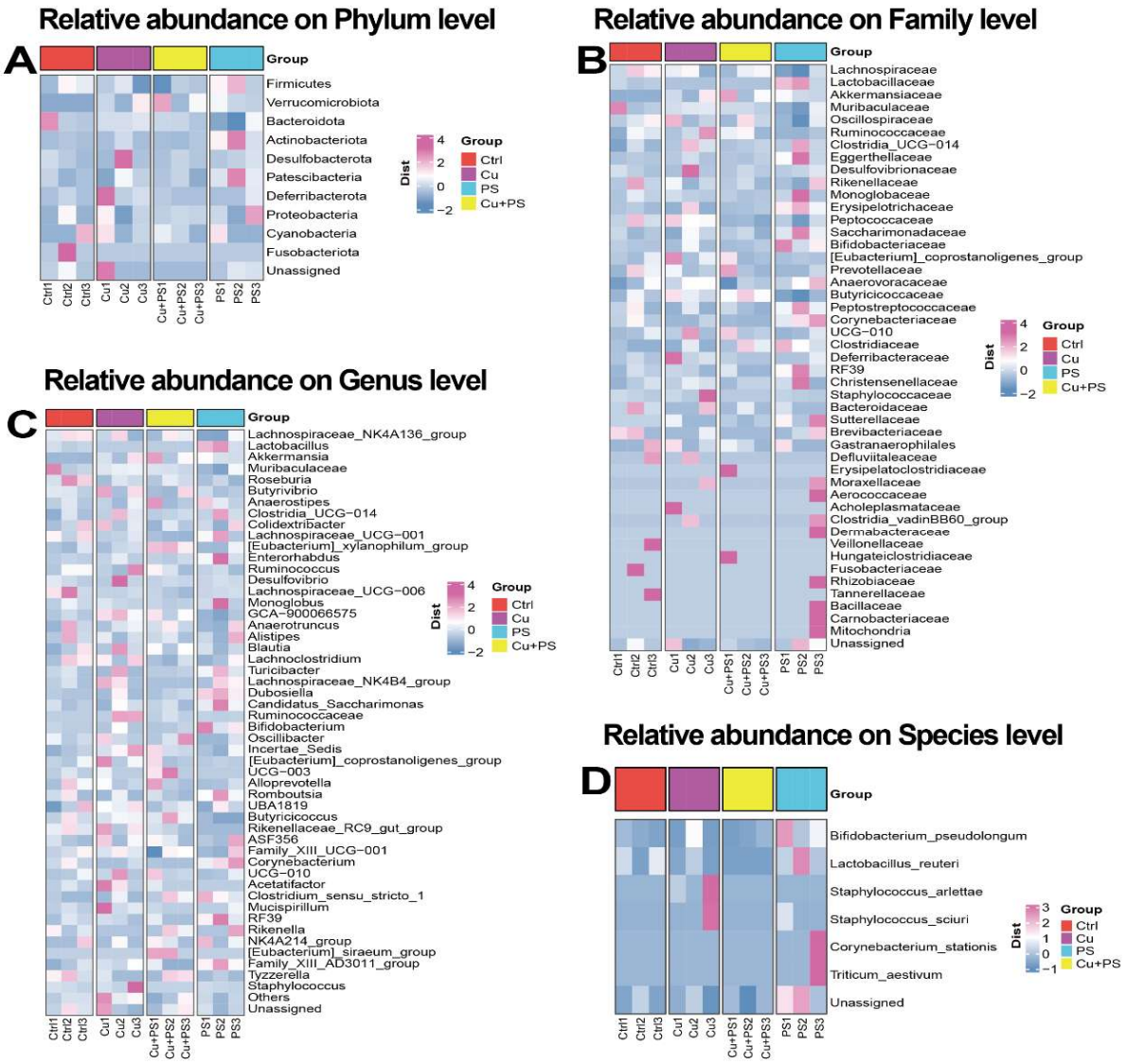

Fig. 5: Heatmap of relative abundance of intestinal microbiota in different treatment groups (phylum/family/genus/species levels). A: Phylum level; B: Family level; C: Genus level; D: Species level differences in microbiota composition.

LEfSe and LDA effect size analysis of intestinal microbiota: The phylogenetic tree and LDA effect size bar plot revealed significantly differentially enriched taxa at multiple taxonomic levels in each group (Fig. 3I-J). The control group was mainly enriched in Roseburia-related taxa; the copper group was significantly enriched in Peptococcales, Peptococcaceae, Rikenellaceae_RC9_gut_ group, and GCA-900066575; the microplastic group was enriched in Bacilli, Lactobacillales, Lactobacillaceae, Lactobacillus, and Corynebacterium; the combined exposure group had fewer differentially enriched taxa, dominated by Butyricicoccaceae.

Differential microbiota analysis based on STAMP: Intergroup differential analysis was conducted at the genus level using STAMP software (t-test, $P<0.05$). As shown in Fig. 6A, the abundances of Unassigned Lachnospiraceae, Unassigned Oscillospiraceae, and Unassigned Ruminococcaceae were significantly lower in the microplastic group compared to the control group. This suggests that microplastics may inhibit the growth of butyrate-producing bacteria and impair the intestinal barrier. Fig. 6B illustrates that the abundances of beneficial bacteria, such as Roseburia, Lachnospiraceae UCG-001, and Rikenellaceae Rc9 gut group, were significantly decreased in the combined exposure group. This indicates that combined exposure can markedly alter the structure of the intestinal microbiota.

As illustrated in Fig. 6C-D, the abundances of Lactobacillus, Roseburia, Lachnospiraceae_UCG-006, and GCA-900066575 were significantly reduced in the copper group compared to the control group. This indicates that copper exposure has altered the composition of the intestinal microbiota. Additionally, as shown in Fig. 6D, the abundances of the [Eubacterium] xylanophilum group, GCA-900066575, Romboutsia, and Dubosiella were noticeably diminished in the combined exposure group compared to the microplastic group. This suggests that combined exposure further reshapes the structure of the intestinal microbiota.

Comparison of predicted KEGG pathway abundance of intestinal microbiota: Significant differences in the functional potential of gut microbiota among groups were observed based on KEGG pathway analysis (R software, $P<0.05$) (Fig. 7). The differential pathways mainly included cancer types, glycan metabolism, bacterial infection, lipid metabolism, and metabolism of cofactors and vitamins. Copper, microplastics alone, and their combined exposure altered the functional distribution of microbiota. Notably, the combined exposure group exhibited significantly increased abundances of glycosphingolipid biosynthesis, biotin metabolism, and lipopolysaccharide biosynthesis pathways, suggesting that combined exposure could further affect microbial metabolic functions and be associated with altered inflammatory-related functions.

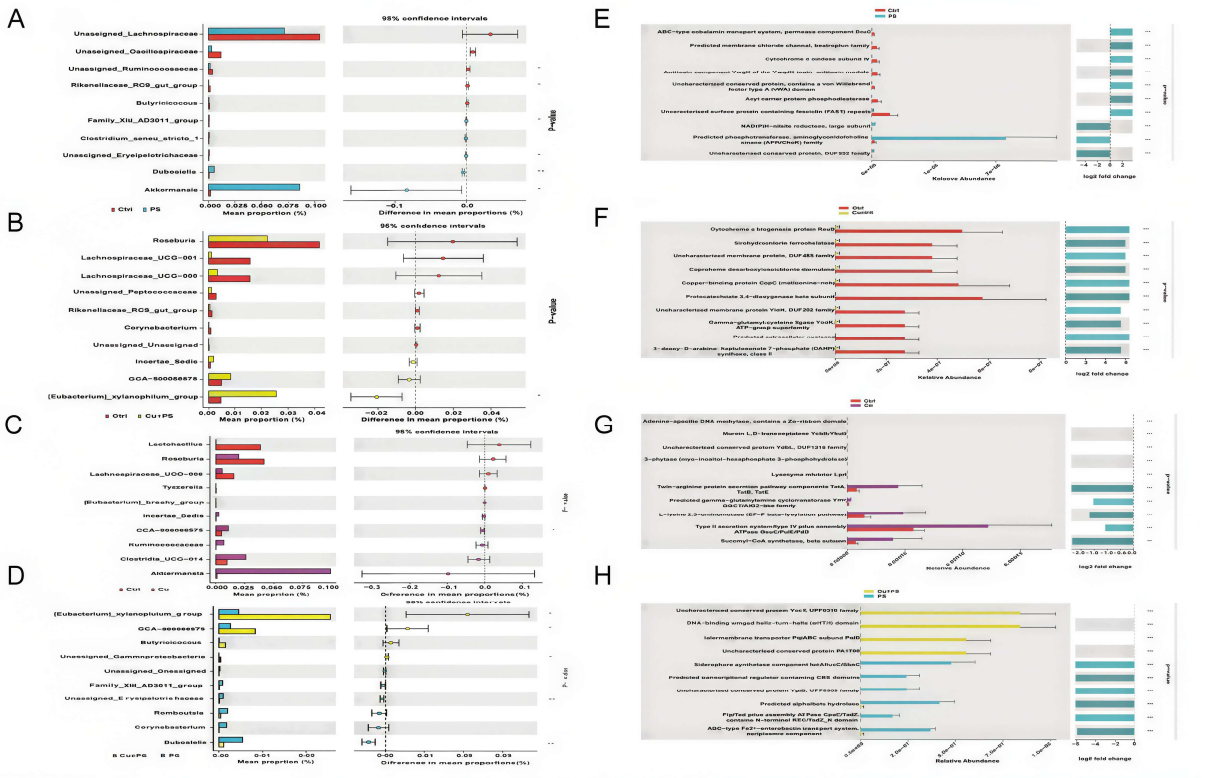

Fig. 6: (A-D) Results of differential microbiota comparison based on STAMP analysis. A: Comparison of differential microbiota between the control group (Ctrl) and the microplastic group (PS); B: Comparison of differential microbiota between the control group (Ctrl) and the combined exposure group (Cu+PS). C: Comparison of differentially abundant taxa between the control group (Ctrl) and the copper-exposed group (Cu); D: Comparison of differentially abundant taxa between the copper + microplastic combined exposure group (Cu+PS) and the microplastic group (PS). (E-H): Comparison of the relative abundance of differentially functional genes in COG/protein families between the control group and various treatment groups. E: Comparison of relative abundance of differentially functional genes between the control group (Ctrl) and the microplastic group (PS); F: Comparison of relative abundance of differentially functional genes between the control group (Ctrl) and the group exposed to both copper and microplastics (Cu+PS). G: Comparison of differential functional genes between the control group (Ctrl) and the copper-exposed group (Cu); H: Comparison of differential functional genes between the combined copper and microplastic exposure group (Cu+PS) and the microplastic group (PS).

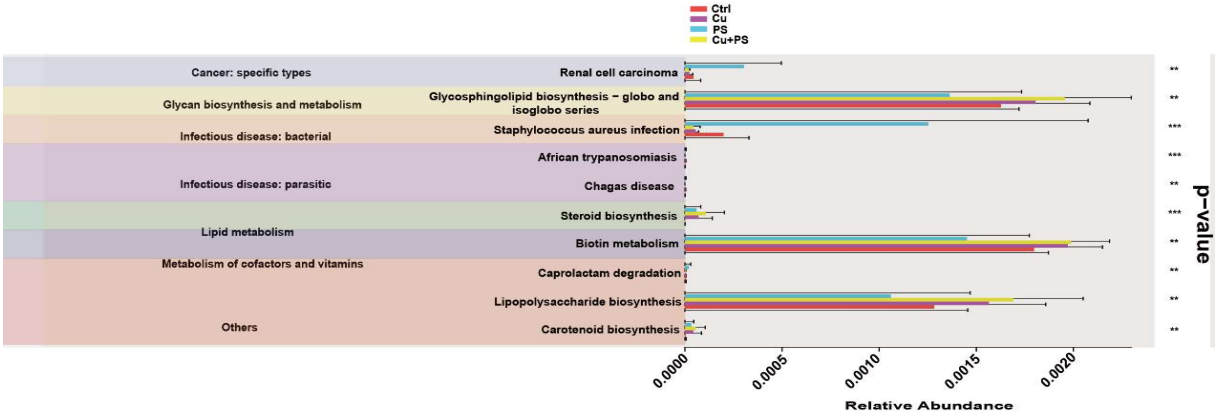

Fig. 7: Comparison of the relative abundance of KEGG pathways predicted by intestinal microbiota function.

Comparison of differentially abundant COG/protein family genes: Based on COG functional annotation analysis, functional differences in intestinal microbiota among groups were identified (Fig. 6E-F). As illustrated in Fig. 6E, the microplastic group demonstrated a reduction in the levels of cytochrome c oxidase subunit IV, vitamin B12 transporter BtuCD, and acyl carrier protein phosphodiesterase compared to the control group. Conversely, there were increased levels of aminoglycoside/choline kinase family proteins and the large subunit of NAD(P)H-nitrite reductase. This suggests that exposure to microplastics affected functions related to energy metabolism, substance transport, and reductive metabolism.

Fig. 6F shows that the control group had higher abundances of γ-glutamylcysteine ligase YbdK, coproporphyrinogen decarboxylase/chlorite dismutase, copper-binding protein CopC, cytochrome c biosynthesis protein ResB, and sirohydrochlorin ferrochelatase than the combined exposure group, suggesting that combined exposure further influenced functions associated with glutathione metabolism, prosthetic group synthesis, metal binding, and electron transport.

In Fig. 6G, it is shown that, compared to the control group, the copper group exhibited significantly increased levels of several components. These include the Twin-arginine protein secretion pathway components (TatA, TatB, TatE), L-lysine 2,3-aminomutase, the EF-P beta-lysylation pathway, the Type II secretion system/type IV pilus assembly ATPases (GspE, PulE, PilB), and Succinyl-CoA synthetase (beta subunit). This suggests that copper exposure can enhance the functional potential of the microbiota related to protein secretion, pilus assembly, and energy metabolism.

The abundances of certain microbial components were lower in the combined-exposure group than in the microplastic group (Fig. 16H). These components include the Flp/Tad pilus assembly ATPase CpaE/TadZ, the siderophore synthetase components IucA/IucC/SbnC, the periplasmic component of the ABC-type Fe^{2+}-enterobactin transport system, and a predicted alpha/beta hydrolase. This suggests that combined exposure inhibits microbial functions related to pilus assembly, iron acquisition, and metabolism.

Effects of combined exposure on differentially expressed genes in the transcriptome

Differential gene clustering heatmap analysis: The gene clustering heatmap was constructed based on the standardized expression levels of differentially expressed genes in each sample, where color changes reflect the relative expression differences of the same gene across different samples (Fig. 8). The results indicated that samples in the same group were generally clustered closely, suggesting good intra-group reproducibility. Meanwhile, distinct expression patterns were observed in multiple gene clusters among different treatment groups, with the most significant expression difference between the combined exposure group and the control group, indicating obvious transcriptional differences between these two groups.

Principal component analysis (PCA) among samples: The results of principal component analysis (PCA) revealed that samples from different treatment groups exhibited a certain separation trend along PC1 and PC2 in the two-dimensional PCA plot, indicating differences in the overall expression profile among groups (Fig. 9A- B). PC1 and PC2 accounted for 31.64 and 18.58% of the total variation, respectively. In the three-dimensional PCA plot with the inclusion of PC3, the spatial distribution differences among groups became more intuitive. PC1, PC2, and PC3 explained 30.52, 18.72, and 13.54% of the total variation, respectively, with the top three principal components cumulatively explaining 62.78% of the variation.

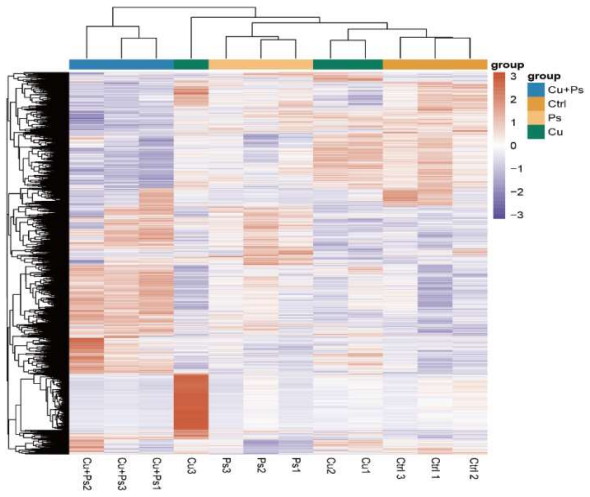

Fig. 8: Clustering heatmap of differentially expressed genes (DEGs). The abscissa represents each group of samples, and the ordinate represents differentially expressed genes (DEGs). The heatmap's color represents the standardized relative expression levels of genes: red indicates high expression, while blue and purple indicate low expression.

Screening and analysis of differentially expressed genes: The volcano plot of differentially expressed genes (DEGs) is presented in Fig. 9C- E. Compared to the control group, a total of 942 DEGs were identified in the copper group, comprising 362 up-regulated and 580 down-regulated genes. In the microplastic group, 1,667 DEGs were detected, with 801 genes up-regulated and 866 down-regulated. The combined exposure group revealed 4,026 DEGs, which included 1,980 up-regulated and 2,046 down-regulated genes. When comparing the single exposure groups, the combined exposure group showed a significant increase in the number of DEGs, and the range of these genes in terms of log2 Fold Change and significance level was broader. This indicates that combined exposure leads to a wider array of transcriptional changes.

Overlap analysis of differentially expressed genes: In Fig. 9F, a Venn analysis of differentially expressed genes (DEGs) was conducted. The total number of DEGs identified in the comparisons of Ctrl vs $CuSO_4$, Ctrl vs PS, and Ctrl vs Cu+PS was 942, 1,667, and 4,026, respectively. Among these comparisons, there were 65 DEGs that were common to all three groups. Notably, the combined exposure group showed 3,226 unique DEGs, which is significantly higher than the 583 unique DEGs found in the copper group and the 905 in the microplastic group. This indicates that combined exposure leads to more specific transcriptional responses that are distinct from those observed with single exposures.

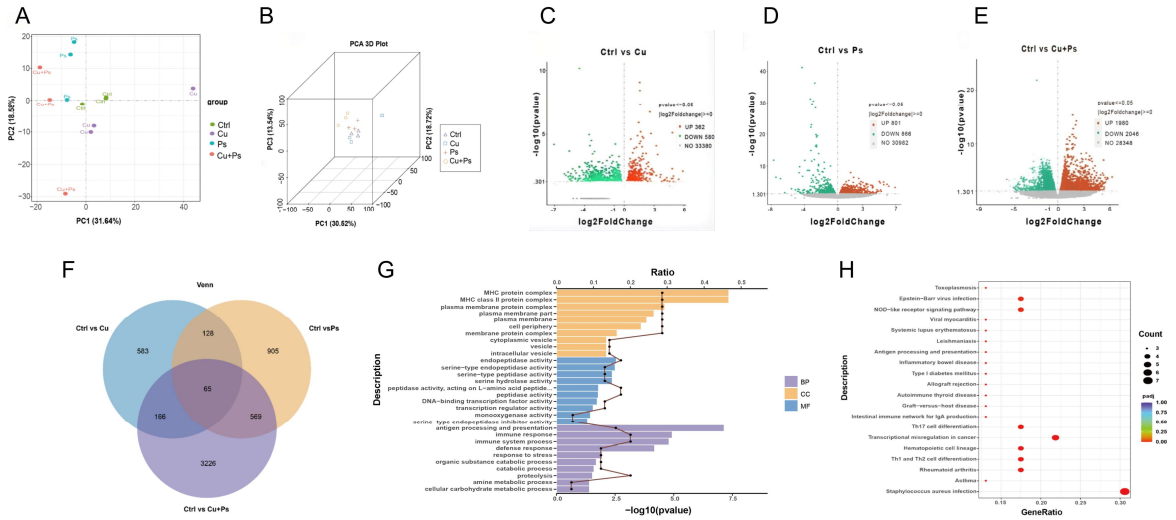

Fig. 9: (A-B) Principal component analysis (PCA) of intestinal transcriptome samples from each treatment group. A: Two-dimensional PCA; B: Three-dimensional PCA. (C-E): Volcano plot of differentially expressed genes in each comparison group. C: Ctrl vs Cu; D: Ctrl vs PS; E: Ctrl vs Cu+PS. Red dots indicate up-regulated genes, green dots indicate down-regulated genes, and gray dots indicate genes with no significant difference. F: Venn diagram of overlapping differentially expressed genes in each comparison group. G: GO enrichment analysis of differentially expressed genes (DEGs). H: KEGG pathway enrichment analysis of differentially expressed genes.

GO enrichment analysis of differentially expressed genes: The results of the GO enrichment analysis, as shown in Fig. 9 G, indicated that differentially expressed genes were primarily enriched in three categories: Biological Process (BP), Cellular Component (CC), and Molecular Function (MF). In the Biological Process category, the main terms included antigen processing and presentation, immune response, immune system processes, defense response, response to stress, and proteolysis. The Cellular Component category focused on components such as the MHC protein complex, MHC class II protein complex, plasma membrane, plasma membrane protein complex, vesicles, and cytoplasmic vesicles. For the Molecular Function category, the key terms included endopeptidase activity, serine-type endopeptidase activity, serine-type peptidase activity, serine hydrolase activity, and transcription regulator activity. Overall, the functional enrichment of the differentially expressed genes was primarily related to immune responses, membrane structural components, and functions associated with proteolysis.

Enrichment analysis of DEGs in KEGG pathways: To elucidate the underlying biological roles of differentially expressed genes (DEGs), we implemented KEGG pathway enrichment analysis (Fig. 9H). The analysis revealed that DEGs were significantly clustered in pathways relevant to immunological and inflammatory mechanisms, encompassing antigen processing and presentation, the intestinal IgA immune network, differentiation of Th1, Th2, and Th17 cells, the NOD-like receptor signaling cascade, and inflammatory bowel disease. Moreover, DEGs were implicated in the pathogenesis of multiple immune-mediated diseases, such as rheumatoid arthritis, asthma, type 1 diabetes mellitus, and systemic lupus erythematosus. Collectively, these findings indicate that DEGs predominantly modulate pathways involved in antigen presentation, T lymphocyte subset differentiation, mucosal immune surveillance, and innate immune inflammatory responses.

DISCUSSION

Intestinal barrier function and microbiota homeostasis are key indicators for evaluating the intestinal toxicity of environmental pollutants. Previous studies have confirmed that intestinal barrier damage can trigger microbial dysbiosis, amplify local inflammatory cascades, and multiple metabolic disorders (Neurath *et al*., 2025). Copper ions can directly disrupt intestinal barrier structure, whereas polystyrene microplastics exacerbate barrier impairment by disturbing the intestinal microenvironment, adsorbing other pollutants, and producing combined adverse impacts (Fontes *et al*., 2024). This study aimed to investigate the effects of exposure to copper and polystyrene microplastics, both individually and in combination, on the mouse intestine.

The intestinal mucosal barrier isolates exogenous harmful substances to maintain host homeostasis, and barrier damage activates mucosal immunity and aggravates inflammation (Di Sabatino *et al*., 2023). The pathological results from this study showed that exposure to either copper or microplastics alone caused mucosal injury. However, the group that was exposed to both pollutants experienced more severe villus atrophy and epithelial shedding. This indicates combined impacts on tissue damage caused by the combination of these two pollutants (Chen *et al*., 2024).

The intestinal epithelial barrier's integrity depends on tight junction stability (Arumugam *et al*., 2025). In this study, the expression levels of ZO-1 and Occludin were significantly downregulated in the combined exposure group, indicating that this exposure markedly disrupts epithelial junction homeostasis and increases intestinal permeability, consistent with previous findings (Ali *et al*., 2025).

Alpha diversity analysis in this study showed that the ACE and Chao1 indices exhibited a downward trend in the copper and microplastic combined exposure group, but the difference was not statistically significant. The Shannon and Simpson indices were significantly higher in the microplastic-only group, indicating a greater impact on community evenness and diversity structure. These results indicate that microplastics do not merely reduce microbial richness but are more likely to induce rearrangement of the microbial community structure. Previous studies have confirmed that polystyrene microplastics can significantly impact the intestinal structure of mice, the expression of tight junction genes, and the composition of intestinal microbiota, which aligns with the findings of the current study (Su *et al*., 2024). Notably, pollutant-induced microbial dysbiosis is not always characterized by reduced alpha diversity; it can also lead to increased Shannon and Simpson indices via the reduction of dominant bacteria and expansion of low-abundance taxa. Therefore, the elevated diversity observed in this study does not reflect improved intestinal health but rather represents a disruption of microbial homeostasis.

The analysis of beta diversity showed significant differences in the structure of microbial communities across all groups. The microplastic-only group was clearly separated from the other groups, while the control, copper-only, and combined exposure groups showed partial overlap, indicating that microplastics exert a more prominent disturbance on the overall microbial structure. Previous studies have confirmed that exposure to microplastics alters the intestinal microbiota structure and impairs barrier function in mice, consistent with our findings (Lu *et al*., 2018). Of note, the combined exposure group did not show the strongest deviation in PCA/PCoA analysis, suggesting that the effects of combined exposure may not necessarily be reflected in maximized overall community distance, but are more likely to involve the remodeling of key microbiota and functional networks. Accordingly, this study further conducted a comprehensive analysis combining differential microbiota and functional prediction.

The main bacterial phyla found in the four groups of mice were Firmicutes, Bacteroidetes, and Verrucomicrobiota; however, their relative abundances differed at the phylum, family, genus, and species levels. The combined exposure group displayed obvious compositional remodeling at multiple taxonomic levels, indicating that copper and microplastics jointly disrupt intestinal microecological balance. Studies have confirmed that microplastic exposure induces abnormal intestinal microbiota structure and damage to the intestinal epithelium and tight junctions in mice (Qiao *et al*., 2021); furthermore, co-exposure to copper and polystyrene nanoplastics can exacerbate intestinal dysfunction and mitochondrial damage (Rong *et al*., 2024), suggesting potential combined toxic effects upon co-exposure. LEfSe and STAMP analyses showed that the abundances of butyrate-producing bacteria, such as Roseburia and Lachnospiraceae, were decreased following microplastic and combined exposure. As butyrate is critical for maintaining intestinal epithelial function and suppressing inflammation (Fu *et al*., 2025), such alterations imply that exposure may weaken intestinal barrier function and increase inflammatory risk (Jin *et al*., 2019). It should be noted that the present microbiome analyses are mainly descriptive, and the direct mechanistic linkage between microbial changes and host intestinal injury remains to be fully elucidated.

Mechanistically, copper damages the barrier by inducing epithelial stress (Djouina *et al*., 2022), while microplastics can directly injure intestinal tissue and tight junctions and act as carriers to enhance the toxicity of other pollutants (Tumwesigye *et al*., 2023); their combination jointly exacerbates intestinal microenvironmental disturbance. Studies have reported that co-exposure to microplastics and cadmium significantly aggravates intestinal barrier damage (Yang *et al*., 2025); these reports are generally consistent with our findings showing complex changes in microbial composition and functional potential in the combined exposure group.

For functional prediction, PICRUSt2 analysis in this study revealed that copper, microplastics, and their combined exposure all affected the potential functional profiles of the intestinal microbiota. KEGG results indicated that the combined exposure group exhibited higher abundances of glycosphingolipid biosynthesis, biotin metabolism, and lipopolysaccharide biosynthesis pathways. COG analysis showed alterations in functional genes related to protein secretion, pilus assembly, energy metabolism, iron acquisition, and reductive metabolism, suggesting that combined exposure not only reshapes microbial structure but also significantly remodels its metabolic and functional potential. These functional predictions generated by PICRUSt2 and KEGG are speculative computational results and have not been validated by experiments. Previous studies have demonstrated that long-term polystyrene microplastic exposure affects intestinal immunity and microecological function in mice (Kuai *et al*., 2024).

Cluster heatmap results indicated good consistency among biological replicates within each group, demonstrating high sample reliability. Venn analysis revealed that the combined exposure group displayed a unique gene expression signature, with a markedly higher number of specifically expressed genes. Differential expression analysis revealed 4026 differentially expressed genes in the combined exposure group, which is significantly more than in the single-exposure groups. This includes a substantial number of unique differentially expressed genes, suggesting that combined exposure leads to more extensive transcriptomic reprogramming (Harusato *et al*., 2023; Shi *et al*., 2024).

GO and KEGG enrichment analyses revealed that the functions of the identified differentially expressed genes were highly consistent. These genes were primarily enriched in immune-related processes, including antigen processing and presentation (MHC-related complexes), mucosal immunity (intestinal IgA network), and T cell differentiation (Th1/Th2, Th17). Additionally, there was significant enrichment in the NOD-like receptor signaling pathway and pathways related to inflammatory bowel disease. Collectively, these bioinformatic results suggest a potential immune regulatory association involving antigen presentation, T cell differentiation, IgA-mediated mucosal defense, and innate immune recognition.

Limitations of the present study should be noted. First, the sample size per group was relatively small (n=6), which

might reduce statistical power and limit the robustness of the current results. In addition, the transcriptomic profiling in this study was based on bioinformatic enrichment analysis without further qPCR validation. The functional predictions derived from GO and KEGG enrichment are preliminary and speculative, and the observed immune-related correlations require further systematic verification in future studies. Therefore, all conclusions in the present study are interpreted cautiously rather than overextended.

Conclusions: The present study concluded that the combined exposure to copper sulfate and polystyrene microplastics significantly increases the risk of intestinal injury and dysfunction in mice. This study presents crucial experimental evidence for clarifying the combined intestinal toxicity mechanisms of environmental pollutants and for conducting relevant risk assessments.

Conflict of interest: The authors declare that they have no competing interests.

Authors contribution: B.X. Lv, H Zhang, and Z.Q. Zhang contributed equally to this study as co-first authors; Y.A. Pan, S. Kang, and M. Chen performed data analysis. B.X. Lv, H Zhang, Z.Q. Zhang, Y.A. Pan. S. Kang, M. Chen, X.Y. Li, F.S. Ataya, and R.B. Luo conducted the investigation, data analysis, and manuscript writing and editing. Z.Y. Chang conceived the study, reviewed and edited the manuscript, and supervised and funded the project.

Funding: This study was supported by the Natural Science Foundation of Xizang Autonomous Region (XZ202401ZR0003), the Science and Technology Programme of Linzhi City, Xizang Autonomous Region (XDHZ-2025-07). The authors extend their appreciation to the Ongoing Research Funding Program (ORF-2026-693), King Saud University, Riyadh, Saudi Arabia.

REFERENCES

Ali Z, Khan I, Iqbal MS, *et al*., 2025. Impact of copper stress in the intestinal barriers and gut microbiota of Chinese stripe-necked turtle (*Mauremys sinensis*). Ecotoxicology and Environmental Safety 290:117723.

Arumugam P, Saha K, Nighot P, 2024. Intestinal epithelial tight junction barrier regulation by novel pathways. Inflammatory Bowel Disease 31:259-271.

Bian S, Zhu S, Li L, *et al*., 2026. Influence of gut microbiota on the metabolism of bovine glycolipids: A review. Microbial Pathogenesis 214:108420.

Bian S, Zhu S, Lu J, *et al*., 2025. Targeting gut microbiota in non-alcoholic fatty liver disease (NAFLD): Pathogenesis and therapeutic insights: A review. International Journal of Biological Macromolecules 330:147995.

Chen X, Xu L, Chen Q, *et al*., 2023. Polystyrene micro and nanoparticles exposure induced anxiety-like behaviors, gut microbiota dysbiosis and metabolism disorder in adult mice. Ecotoxicology and Environmental Safety 259:115000.

Chen Y, Zeng Q, Luo Y, *et al*., 2024. Polystyrene microplastics aggravate radiation-induced intestinal injury in mice. Ecotoxicology and Environmental Safety 283:116834.

Dai J, Yang X, Yuan Y, *et al*., 2020. Toxicity, gut microbiota and metabolome effects after copper exposure during early life in SD rats. Toxicology 433-434:152395.

Di Sabatino A, Santacroce G, Rossi CM, *et al*., 2023. Role of mucosal immunity and epithelial-vascular barrier in modulating gut homeostasis. Internal and Emerging Medicine 18:1635-1646.

Djouina M, Vignal C, Dehaut A, *et al*., 2022. Oral exposure to polyethylene microplastics alters gut morphology, immune response, and microbiota composition in mice. Environmental Research 212:113230.

Fontes A, Pierson H, Bierła JB, *et al*., 2024. Copper impairs the intestinal barrier integrity in Wilson disease. Metabolism 158:155973.

Fu L, Wang M, Li D, *et al*., 2025. Microbial metabolites short chain fatty acids, tight junction, gap junction, and reproduction: a review. Frontiers in Cell and Developmental Biology 13:1624415.

Harusato A, Seo W, Abo H, *et al*., 2023. Impact of particulate microplastics generated from polyethylene terephthalate on gut pathology and immune microenvironments. iScience 26:106474.

Hou J, Wu P, Cai J, *et al*., 2025. Gut microbiota dysbiosis amplifies thiram hepatotoxicity via a mitochondrial-autophagy-apoptosis nexus orchestrated by the gut-liver axis. Cell Signal 136:112104.

Hu L, Feng X, Lan Y, *et al*., 2024. Co-exposure with cadmium elevates the toxicity of microplastics: Trojan horse effect from the perspective of intestinal barrier. Journal of Hazardous Materials 466:133587.

Huang D, Zhang Y, Long J, *et al*., 2022. Polystyrene microplastic exposure induces insulin resistance via dysbacteriosis and pro-inflammation. Science of Total Environment 838:155937.

Jin Y, Lu L, Tu W, *et al*., 2019. Impacts of polystyrene microplastic on the gut barrier, microbiota and metabolism of mice. Science of Total Environment 649:308-317.

Kuai Y, Chen Z, Xie K, *et al*., 2024. Long-term exposure to polystyrene microplastics reduces macrophages and affects the microbiota-gut-brain axis in mice. Toxicology 509:153951.

Li Y, Liu K, Li Y, *et al*., 2026. The gut microbiota-derived metabolites regulate bone extracellular matrix homeostasis: Mechanisms and therapeutic implications. Cell Signal 138:112245.

Liang B, Zhong Y, Huang Y, *et al*., 2021. Underestimated health risks: polystyrene micro- and nanoplastics jointly induce intestinal barrier dysfunction by ROS-mediated epithelial cell apoptosis. Particle and Fibre Toxicology 18:20.

Liu Y, Zhang S, Deng H, *et al*., 2023. Lead and copper influenced bile acid metabolism by changing intestinal microbiota and activating farnesoid X receptor in Bufo gargarizans. Science of Total Environment 863:160849.

Lu L, Wan Z, Luo T, *et al*., 2018. Polystyrene microplastics induce gut microbiota dysbiosis and hepatic lipid metabolism disorder in mice. Science of Total Environment 631-632:449-458.

Lv W, Shen Y, Xu S, *et al*., 2023. Underestimated health risks: Dietary restriction magnify the intestinal barrier dysfunction and liver injury in mice induced by polystyrene microplastics. Science of Total Environment 898:165502.

Neurath MF, Artis D, Becker C, 2025. The intestinal barrier: a pivotal role in health, inflammation, and cancer. Lancet Gastroenterology and Hepatology 10:573-592.

Qiao J, Chen R, Wang M, *et al*., 2021. Perturbation of gut microbiota plays an important role in micro/nanoplastics-induced gut barrier dysfunction. Nanoscale 13:8806-8816.

Rong J, Yuan C, Yin X, *et al*., 2024. Co-exposure of polystyrene nanoplastics and copper induces development toxicity and intestinal mitochondrial dysfunction *in-vivo* and *in-vitro*. Science of Total Environment 930:172681.

Shen W, Zhao M, Xu W, *et al*., 2024. Sex-specific effects of polystyrene microplastic and Lead(II) co-exposure on the gut microbiome and fecal metabolome in C57BL/6 mice. Metabolites 14(4):189.

Shi J, Yu X, Zhao J, *et al*., 2024. Integrated transcriptomics and metabolomics reveal the mechanism of polystyrene nanoplastics toxicity to mice. Ecotoxicology and Environmental Safety 284:116925.

Su Q, Wu J, Tan S, *et al*., 2024. The impact of microplastics polystyrene on the microscopic structure of mouse intestine, tight junction genes and gut microbiota. PLoS One 19:e0304686.

Tang Y, Wu X, Pang Y, *et al*., 2024. Toxicity of Polystyrene microplastics with Cadmium on the digestive system of *Rana zhenhaiensis* tadpoles. Toxics 12(12):854.

Tumwesigye E, Nnadozie CF, Akamagwuna FC, *et al*., 2023. Microplastics as vectors of chemical contaminants and biological agents in freshwater ecosystems: Current knowledge status and future perspectives. Environmental Pollution 330:121829.

Wen S, Zhao Y, Liu S, *et al*., 2022. Polystyrene microplastics exacerbated liver injury from cyclophosphamide in mice: Insight into gut microbiota. Science of Total Environment 840:156668.

Wu J, Wen XW, Faulk C, *et al*., 2016. Perinatal Lead exposure alters gut microbiota composition and results in sex-specific bodyweight increases in adult mice. Toxicological Sciences 151:324-333.

Yang J, Wang D, Huang J, *et al*., 2025. Intestinal barrier disruption by Cadmium and microplastics: Mechanistic insights from integrated metabolomic and proteomic analysis in mice. Environmental Pollution 382:126696.

Yang Y, Chi L, Liu C, *et al*., 2023. Chronic Arsenic exposure perturbs gut microbiota and bile acid homeostasis in mice. Chemical Research in Toxicology 36:1037-1043.

Zhang Z, Xu M, Wang L, *et al*., 2023. Continuous oral exposure to micro- and nanoplastics induced gut microbiota dysbiosis, intestinal barrier and immune dysfunction in adult mice. Environment International 182:108353.

Zhu Q, Chen B, Zhang F, *et al*., 2024. Toxic and essential metals: metabolic interactions with the gut microbiota and health implications. Frontiers in Nutrition 11:1448388.

Zhu S, Bian S, Lu J, *et al*., 2026. Pathogenesis of Bovine Mastitis and Influence of the Gut Microbiota: A Review. Journal of Agricultural and Food Chemistry 74(5):4222-4234.